Atmospheric Environment 244 (2021) 117883

Contents lists available at ScienceDirect

Atmospheric Environment

journal homepage: http://www.elsevier.com/locate/atmosenv

# Stage-resolved in-cloud scavenging of submicron and BC-containing particles: A case study

Yuxiang Yang [a,b], Qinhao Lin [a,f], Yuzhen Fu [a,b], Xiufeng Lian [a,b], Feng Jiang [a], Long Peng [a,b], Guohua Zhang [a], Lei Li [c], Duohong Chen [d], Mei Li [c], Jie Ou [e], Xinhui Bi [a,*], Xinming Wang [a], Guoying Sheng [a]

[a] State Key Laboratory of Organic Geochemistry and Guangdong Key Laboratory of Environmental Protection and Resources Utilization, Guangzhou Institute of Geochemistry, Chinese Academy of Sciences, Guangzhou 510640, PR China
[b] University of Chinese Academy of Sciences, Beijing 100039, PR China
[c] Atmospheric Environment Institute of Safety and Pollution Control, Jinan University, Guangzhou 510632, PR China
[d] State Environmental Protection Key Laboratory of Regional Air Quality Monitoring, Guangdong Environmental Monitoring Center, Guangzhou 510308, PR China
[e] Shaoguan Environmental Monitoring Center, Shaoguan 512026, PR China
[f] Now at: Guangdong Key Laboratory of Environmental Catalysis and Health Risk Control, School of Environmental Science and Engineering, Institute of Environmental Health and Pollution Control, Guangdong University of Technology, Guangzhou 510006, PR China

## HIGHLIGHTS

- The stage-resolved scavenging efficiency of BC particles is firstly reported.
- Scavenging efficiency (SE) is dominantly controlled by liquid water content (LWC).
- Key factors influencing the in-cloud SE of BC-containing particles are assessed.

## ARTICLE INFO

*Keywords:*
Black carbon
In-cloud scavenging
Scavenging efficiency
Liquid water content
Particle size
Mixing state

## ABSTRACT

Interactions between clouds and black carbon (BC) represent a significant uncertainty in aerosol radiative forcing. To investigate the influence of cloud processing on the scavenging of BC, concurrent measurement of individual cloud droplet residue particles (cloud RES) and interstitial particles (cloud INT) throughout a cloud event was deployed at Mt. Tianjing (1690 m a.s.l.) in southern China. An aethalometer (AE-33), a single particle aerosol mass spectrometer (SPAMS) and a scanning mobility particle sizer (SMPS) were used to investigate the mass concentration of equivalent BC (EBC), size-resolved number of BC-containing particles, and size-resolved number concentration of submicron particles in real-time, respectively. The number-based SEs of the submicron particles varied between 2.7 and 31.1%. Mass scavenging efficiency (MSE) ranged from 4.7% to 52.6% for EBC, consistent with the number-based SE (from 11.3% to 59.6%) of the BC-containing particles throughout the cloud event. Several factors that may influence the SEs of the BC-containing particles are considered and examined. SEs are most likely determined by a single factor, i.e., liquid water content (LWC), with $R^2 > 0.8$ in a power function throughout the cloud event. Stage-resolved investigation of SEs further reveals that particle size matters more than other factors in the cloud formation stage, whereas there is an increasing role of the mixing state in the development and stability stage. We also observed lower SEs for the BC-containing particles internally mixed organics, consistent with previous literature.

## 1. Introduction

Primarily originating from incomplete combustion of fossil fuel and biomass, black carbon (BC) shows remarkable impacts on global climate (Bond et al., 2013; Koch and Del Genio, 2010; Nordmann et al., 2014). BC can be removed via dry deposition and wet scavenging, including

* Corresponding author.
*E-mail address:* bixh@gig.ac.cn (X. Bi).

https://doi.org/10.1016/j.atmosenv.2020.117883
Received 9 February 2020; Received in revised form 6 August 2020; Accepted 23 August 2020
Available online 6 September 2020

in-cloud and below-cloud processes. On a global scale, wet scavenging towards the ocean surface is five folds higher than dry deposition for BC aerosols (Jurado et al., 2008). Previous studies have shown that BC is ubiquitous in liquid cloud (Bi et al., 2016; Lin et al., 2017; Liu et al., 2018) and below-cloud processes usually contribute smaller in particle scavenging (Emerson et al., 2018; Ervens, 2015).

In-cloud scavenging mechanisms are generally represented as impaction/coagulation and nucleation (Ervens, 2015). Impaction/coagulation scavenging dominates in a size range of ≤50 nm whereas nucleation plays a crucial role for larger size particles (>140 nm) (Hoose et al., 2008; Levin et al., 2003). Croft et al. (2016) found that the coagulation/impaction scavenging sharply lower the number concentration of particles smaller than 200 nm. Taking this mechanism into account, the number concentration of particles larger than 10 nm would decrease 15–21% globally, whereas particles larger than 80 nm (a proxy for cloud condensation nuclei, CCN) only drop 10–12% (Pierce et al., 2015). Although numerous studies stated that nucleation is the dominating scavenging mechanism for BC (Schroder et al., 2015; Taylor et al., 2014), Baumgardner et al. (2008) revealed that impaction/coagulation is of great importance to scavenge BC in upper tropospheric or cirrus cloud.

Scavenging efficiency (SE), defined as the mass/number fraction (MSE or NSE) of components in cloud droplets, reflecting the ability of species to form cloud droplets.

$$SE = \frac{C_{RES}}{C_{RES} + C_{INT}} \times 100\% \quad (1)$$

where $C_{RES}$ and $C_{INT}$ denote the mass or number concentration of BC or detected number of BC-containing particles in cloud droplet residues (RES) and interstitial particles (INT), respectively.

Most current studies focused on the mean MSE of BC (Herckes et al., 2013; Yang et al., 2019). The reported MSEs varied from 6% at urban city (Hallberg et al., 1992) to ~ 80% at a remote marine site near the Arctic (Heintzenberg and Leck, 1994), showing significant regional discrepancies ((Yang et al., 2019) and references therein). For NSE, Zhang et al. (2017) reported a 5–45% of NSE at Mt. Tianjing, southern China, while the NSE was only 1–10% for BC at Mt. Jungfraujoch (Schroder et al., 2015). Ding et al. (2019) found that 80% of BC-containing particles were removed through coagulation in mixed-phase cloud at the north of Taihang ridge. The discrepancy may originate from the cloud types (liquid, mixed-phase, or ice cloud) and the environmental conditions.

The metrological conditions, including supersaturation of water vapor, liquid water content (LWC), temperature, and physicochemical properties of BC (e.g., size, mixing state, thickness of coating, chemical composition, and so forth), play complex roles in the SE of BC (Browse et al., 2012; Ching et al., 2012; Cozic et al., 2007; Moteki et al., 2012; Motos et al., 2019b; Ohata et al., 2016; Schroder et al., 2015; Zhang et al., 2017). Generally, SE increases with growing particle size, LWC, and supersaturation (Ching et al., 2018; Hitzenberger et al., 2001; Matsui, 2016; Motos et al., 2019a; Sellegri et al., 2003; Wu et al., 2019). Nevertheless, key factors and mechanisms remain ambiguous and may differ under various conditions. Zhang et al. (2017) revealed that mixing state is the key factor in in-cloud scavenging of BC under low LWC conditions (<0.1 g $m^{-3}$). An investigation in Chile revealed that the MSE of BC varied dramatically (13–50%) with different air masses (Heintzenberg et al., 2016).

Considering the ever-changing environmental conditions, understanding the evolution of SE of BC in a cloud event is crucial to evaluate their impacts on climate properly. Targino et al. (2009) found that the SE of aerosol particles at the Mt. Åreskutan in Swedish is not identical even in just one day during a cloud event. By and large, a cloud event can be divided into stages including formation, development, stability and dissipation (Dupont et al., 2012; Koracin et al., 2005).

Therefore, the aims of the present study are (1) to reveal a more detailed evolution of the SE of BC throughout a complete cloud event, (2) to recognize the key factors influencing the in-cloud scavenging of BC particles in different stages. Besides, discrepancies between BC-containing and submicron particles are also discussed.

## 2. Method

### 2.1. General characterization

Field observation was carried out from 30 May to 3 Jun 2017. The sampling site is located in National Air Background Monitoring Station at Mt. Tianjing (112°53′56″ E, 24°41′56″ N; 1690 m a.s.l.) in southern China (Lin et al., 2017). It is surrounded by a national forest park (273 $km^2$) and scarcely affected by anthropogenic activities.

During the sampling period, southwestern air mass was dominated (Fig. S1 in the Supplementary Material). The cloud event, identified by a ground-based counterflow virtual impactor (GCVI), started at 19:00 on 30 May and ended at 14:00 on 3 Jun, was marked by black rectangle in Fig. 1. The hill cap cloud we focused on is likely to be a product of orographic lifting of air parcels. The cloud event was roughly divided into three stages based on estimated LWC (Table 1) similar to Motos et al. (2019a). Other parameters (e.g., vapor pressure (~830 hPa), temperature, RH) didn't show remarkable variations during the cloud event (Fig. 1). While there are other microphysical parameters (e.g., cloud-base height, cloud reflectivity, Doppler velocity) used in other studies (Dupont et al., 2012; Koracin et al., 2005), they are not available in the present study. Here, the formation stage and dissipation stage were characterized by low LWC (<0.1 g $m^{-3}$), and the development and stability stage by LWC higher than 0.1 g $m^{-3}$. The time periods for three cloud stages are: (1) formation (from 19:00 on 30 May to 12:00 on 31 May), (2) development and stability (from 17:00 on 31 May to 20:00 on 2 Jun), and (3) dissipation (from 20:00 on 2 Jun to 14:00 on 3 Jun), respectively.

The trend of the mass concentration of $PM_{2.5}$ indicated that it can be used as a supporting parameter to divide cloud stages. At the cloud formation stage, the mass concentration of $PM_{2.5}$ decreased from 75.9 μg $m^{-3}$ to 0.5 μg $m^{-3}$ from 19:00 on 30 May to 07:00 on 31 May and rebounded back to 39.1 μg $m^{-3}$ until 17:00 on 31 May. When it came to the development and stability stage, $PM_{2.5}$ was effectively scavenged and remained at a low level (<4 μg $m^{-3}$), whereas a weak bounce to 15.8 μg $m^{-3}$ at 11:00 on 3 Jun was observed when the cloud event tended to dissipate.

### 2.2. Instrumentation

In the present study, particles were introduced into the instruments via two parallel sampling inlets. Cloud residue particles (cloud RES) were sampled by GCVI while cloud INT and ambient (cloud-free) particles by a $PM_{2.5}$ cutoff. A timer switch was connected between sampling inlets and parallelly-connected downstream instruments to measure cloud RES and INT alternately with identical time episodes. Fig. S2 shows a schematic plot of the instrument connections.

The GCVI (model 1205, Brechtel Mfg., Inc., USA) was applied to collect cloud droplet, larger than a certain cut size (Lin et al., 2017), at which the transmission efficiency (TE) is 50%. The size is set to be larger than 8.5 μm in the present study. The collected droplets are subsequently dried in an evaporation chamber (with an airflow temperature at 40 °C), leaving residues to be analyzed by downstream instruments. The GCVI employs a compact wind tunnel upstream of the CVI inlet to accelerate cloud droplets into the CVI inlet tip, resulting in an enhancement of collected droplets (Shingler et al., 2012). The mass and number concentrations that measured quantitatively were calibrated by such enhancement (Lin et al., 2017). An upper limit visibility threshold of 3 km and a lower-limit relative humidity (RH) threshold of 95% were set in the GCVI software to identify the presence of cloud events and trigger the sampling of the cloud RES particles.

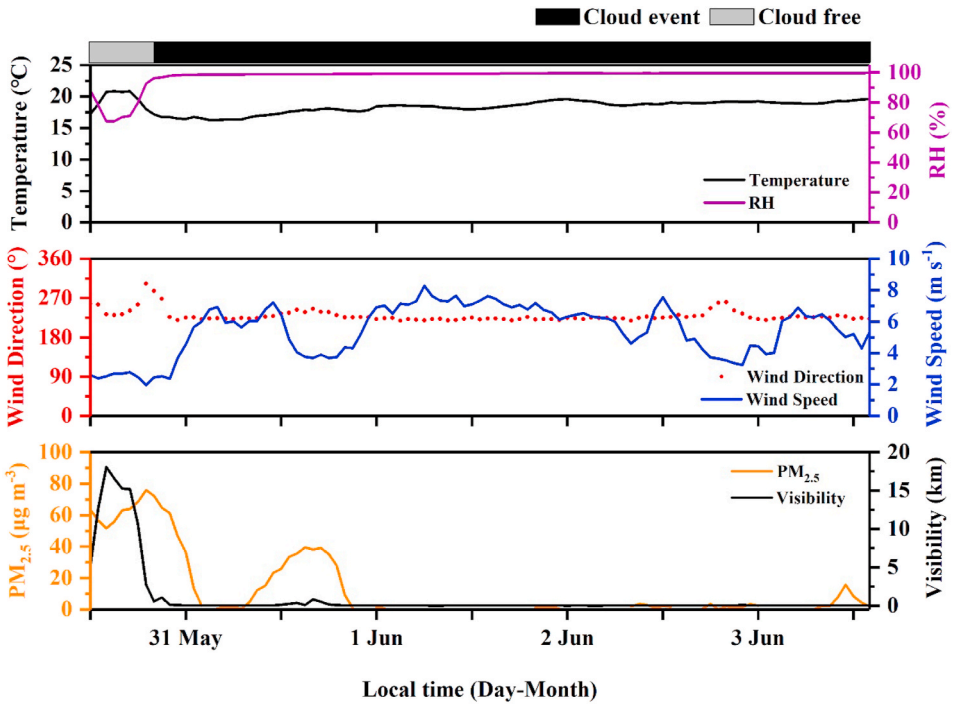


**Fig. 1.** Time series of hourly average values of metrological parameters (temperature, relative humidity (RH), wind direction, wind speed, visibility), and $PM_{2.5}$. During the sampling period, the temperature and RH generally varied between 16.3 and 20.9 °C and 67.5–99.8%, respectively. Before the cloud formed, the RH increased from 71.1% to 92.6% and visibility decreased from 15.1 km to 2.7 km rapidly within 3 h. Throughout the cloud event, $PM_{2.5}$ was significantly scavenged.

**Table 1**
Variation of LWC during the cloud event.

| Sampling period | LWC (g $m^{-3}$) |
|---|---|
| 19:00, 30 May – 12:00, 31 May | 0.03 |
| 0:00–7:40, 1 Jun | 0.13 |
| 7:40–11:00, 1 Jun | 0.29 |
| 11:00, 1 Jun – 1:00, 2 Jun | 0.22 |
| 1:00–9:00, 2 Jun | 0.13[a] |
| 9:00–20:30, 2 Jun | 0.15 |
| 20:30 2 Jun – 14:00, 3 Jun | 0.08 |

[a] The online data was not available during the period.

Aethalometer (model AE-33, Magee Scientific., USA) measures the variation of mass concentration of BC by determining the variation of light absorption at the wavelength of 880 nm, which is typically represented as equivalent BC (EBC) (Petzold et al., 2013). Given the "filter loading effect" in BC measurement, AE-33 compensates the light attenuation utilizing dual spot technology (Drinovec et al., 2015).

A scanning mobility particle sizer (SMPS, MSP Cooperation) was used to measure the size distribution of submicron particles (20–620 nm, electrical mobility diameter, $D_m$). Although most studies measure CCN by cloud condensation nuclei counter (CCNC) (Motos et al., 2019a; Psichoudaki et al., 2018), particles measured by SMPS during cloud RES sampling can represent CCN for numerous CCN distribute in submicron range.

The vacuum aerodynamic diameter ($D_{va}$) and the chemical compositions of the individual particles were analyzed by single particle aerosol mass spectrometer (SPAMS, Hexin Analytical Instrument Co., Ltd.). Detailed instrumentations can be found in Supplementary Material and a detailed description of the performance and the calibrations of the SPAMS can be found elsewhere (Li et al., 2011). The mass spectra for ~130000 cloud RES particles and 70000 INT particles with $D_{va}$ values in the range of 0.1–2.0 μm were obtained by the SPAMS throughout the cloud event. The average number fractions of BC-containing particles in the cloud RES and INT particles were 77.3% and 78.8%, respectively.

An active strand cloud water collector (CASCC2) was used to collect cloud water. Detailed procedures of cloud water collection can be found elsewhere (Demoz et al., 1996; Guo et al., 2012). Briefly, the air is introduced into the rectangular inlet via the suction force provided by the downstream fan. The cloud water droplets are condensed on the Teflon strands, which are inclined at 35° from vertical and then flow into a 250 mL polyethylene (PE) bottle through the connected Teflon tube. The bottle was weighted by a balance before and after sampling to obtain the mass of the cloud water. The value of LWC (g $m^{-3}$) then could be roughly estimated (Guo et al., 2012).

$$LWC = \frac{M}{T \times V_{air} \times \eta} \quad (2)$$

where $M$ is the mass of the cloud water (g), $T$ is the time period of sampling (min), $V_{air}$ and $\eta$ are air volume rate (5.8 $m^3$ $min^{-1}$) and collection efficiency (0.86) of CASCC2, respectively (Demoz et al., 1996).

### 2.3. Different types of BC-containing particles

Particles detected by SPAMS were firstly classified by an adaptive resonance theory neural network algorithm (ART-2a) method based on the presence and intensities of ion peaks and then combined manually. BC-containing particles were characterized with obvious carbon cluster ions in the positive/negative mass spectrum. Three types of BC-containing particles were identified based on the similar criteria in our previous study (Zhang et al., 2017): (a) BC-Sul1: the mass spectra of particles with more carbon cluster ions ($C_n^{\pm}$, n > 5) and sulfate ($m/z$ −97 $HSO_4^-$); (b) BC-Sul2: those with obvious carbon cluster ions ($C_n^{\pm}$, n ≤ 5, but more pronounced in positive mass spectrum) and remarkable sulfate and nitrate ($m/z$ −62 $NO_3^-$, and $m/z$ −46 $NO_2^-$), and (c) BC-OC-Sul: those with an abundance of both sulfate and obvious fragment ions of organics ($m/z$ 27 $C_2H_3^+$, $m/z$ 37 $C_3H^+$, $m/z$ 43 $C_2H_3O^+$, $m/z$ −26 $CN^-$, etc.). Type BC-Sul2 dominated in the three types of BC-containing particles (>95% on average by number) (Fig. S3).

## 3. Results and discussion

To characterize the evolution of SEs, Fig. 2 displays the time series of (a) number concentration and NSE of submicron particles by SMPS, (b) mass concentration and MSE of EBC by AE-33 and (c) number concentration and NSE of BC-containing particles by SPAMS, respectively. Three kinds of SEs show a similar trend with the cloud stages. In the formation stage of the cloud event, visibility dropped dramatically from 18 km to 200 m and bounced back to 800 m at about 12:00 on 31 May. In the development and stability stage, the SEs gradually increased and then kept stable as the highest. The SEs reduced gradually during the dissipation stage.

### 3.1. Stage-resolved in-cloud scavenging of submicron particles during the cloud event

The number concentration of submicron particles in cloud RES and INT are in ranges of 86–522 $cm^{-3}$ and 602-3286 $cm^{-3}$, respectively (Fig. 2 (a)). NSEs of submicron particles were in a variety of 2.7–31.1%, with a mean value of 17.2% throughout the cloud event. The stage-averaged NSEs for submicron particles are 9.4% for the formation stage, 21.1% for the development and stability stage and 15.1% for the dissipation stage, respectively.

The variations of stage-resolved of NSEs with size-resolved submicron particles are shown in Fig. 3. Since the variations are quite similar after the formation stage of the cloud, we merged data of these two stages (the development and stability stage and the dissipation stage), as "after-formation stage" here. The NSEs decrease from 20 nm to 50 nm and then increase gradually in rest size bins, quite similar to that observed at Mt. Åreskutan in Swedish (Targino et al., 2007). They revealed a parabolic-like relationship between SE of bulk aerosols and size during a cloud event, indicating size-dependent scavenging mechanisms (Hoose et al., 2008; Levin et al., 2003). For 20–50 nm particles, the decreasing NSE could be attributed to the decreasing effect of coagulation/impaction, whereas the increasing NSE towards larger particles (for particles larger than 50 nm) suggests the increasing effect of nucleation (Hoose et al., 2008). The lowest SEs for particles in ~40–50 nm may be a result of weak impacts from both scavenging mechanisms. However, the inflection size slightly varies with the cloud stages, with the lowest NSEs at 50 nm and 38 nm for the formation stage and after-formation stage, respectively. The decreasing of the inflection sizes reflects a lower critical activation (nucleation) diameter at higher LWC (Table 1) (Henning et al., 2002). This is also supported by fitting the size-resolved NSEs of submicron particles versus LWC, according to a power function ($NSE = a \times LWC^b$), as shown in Fig. S4. The fitting indicates that the NSEs of the 30–50 nm particles are independent on LWC, while the NSEs in other size bins generally increase with LWC. This phenomenon may also indicate that both the coagulation/impaction scavenging of the 20–30 nm particles and the nucleation scavenging of >50 nm particles could be well predicted with LWC.

### 3.2. Stage-resolved in-cloud scavenging of BC-containing particles

As shown in Fig. 2 (b) and (c), the mass concentration of BC varies from 0.032 μg $m^{-3}$ to 0.37 μg $m^{-3}$ in cloud RES and from 0.083 μg $m^{-3}$ to 1.32 μg $m^{-3}$ in cloud INT. The MSE and NSE varies from 4.7% to 52.6% and 11.3%–59.6%, with a mean value of 35.1% and 37.3%, respectively. The results are quite similar to our previous study at the same site (Zhang et al., 2017). The mean MSE is also comparable to other studies in regions with similar altitudes (Acker et al., 2002; Sellegri et al., 2003). Generally, the MSE of EBC increases with the increase of altitude, which may be a result of the hygroscopic aging of BC-containing particles (Yang et al., 2019). The lowest MSE and NSE of BC with a mean value of 17.3% and 15.4% were observed at the formation stage. In the development and stability stage, the average MSE and NSE increase to 42.5% and 45.3% while the values decreased to 33.7% and 37.6% in the dissipation stage. Furthermore, it is noted that the NSE of BC was much higher than NSE of submicron particles, which could be explained by the fact that a lot of small submicron particles with low NSE cannot be detected by SPAMS. Detailed comparison of size distributions between the two instruments could be found in Supplementary Material (Fig. S5).

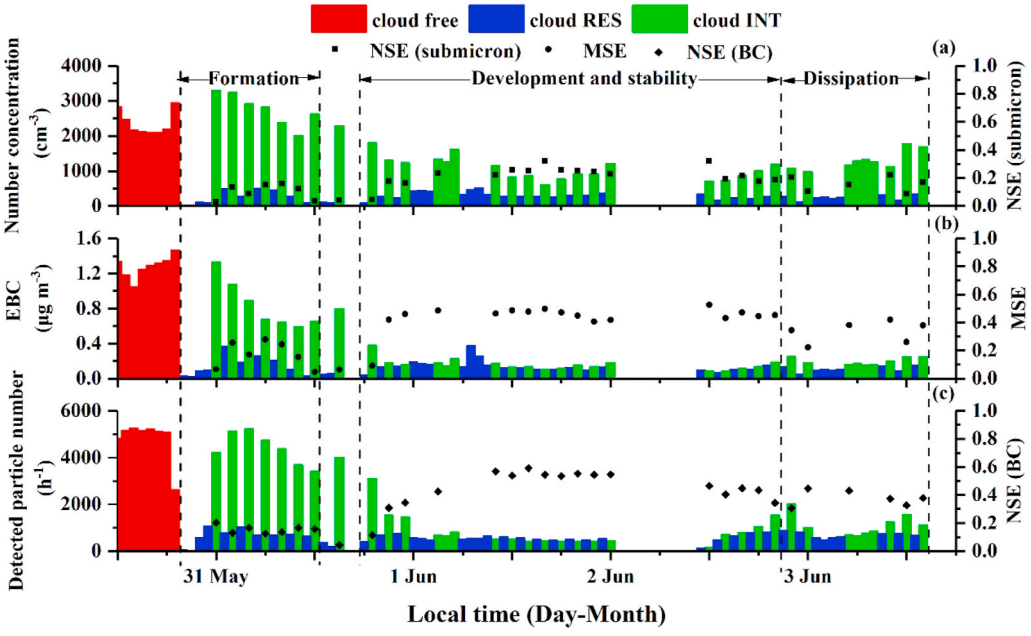


**Fig. 2.** Time series of SEs for (a) number concentration of submicron particles, (b) mass concentration of EBC and (c) detected number of BC-containing particles, respectively. Dash lines are used to separate each period, which are marked as Formation, Development and stability, and Dissipation, respectively. From 12:00 to 17:00 on 31 May, the cloud was unstable and thus the data was not divided into any stage.

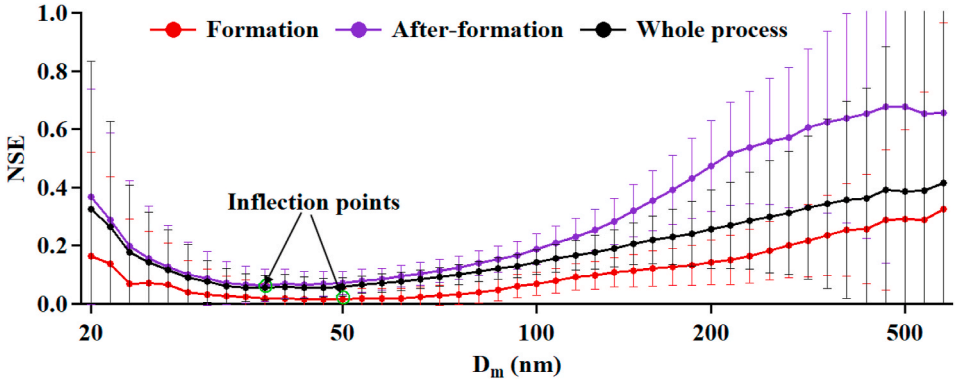


**Fig. 3.** Submicron particle NSE as a function of $D_m$ for each stage and the whole cloud event while After-formation denotes a combination of data of both the development and stability stage and the dissipation stage. The green blank circles are used to mark the inflection points of the curves. (For interpretation of the references to color in this figure legend, the reader is referred to the Web version of this article.)

### 3.3. Influencing factors on SE of BC-containing particles

#### 3.3.1. LWC and concentration of unactivated particles

To investigate the relationship between LWC and SE, Fig. 4 shows the relationships between LWC and SEs of different types of BC-containing particles after a power fitting ($SE = a \times LWC^b$). It can be seen that SEs showed a strong correlation with LWC for EBC, and all types of BC-containing particles ($R^2 > 0.8$). This result is in accordance with the result obtained at Mt. Jungfraujoch (Cozic et al., 2007), where there is an exponential increasing relationship between SE and LWC. Besides, Hitzenberger et al. (2000) revealed a log-linear increasing relationship between them at Mt. Sonnblick. As reported in many previous studies, the influence of LWC on SE of BC would somewhat reach a plateau and keep flat at a threshold (Cozic et al., 2007; Hitzenberger et al., 2001; Hitzenberger et al., 2000; Kasper-Giebl et al., 2000), the decreasing slope (ΔSE/ΔLWC) of the fitting curves may indicate the similar trend (Fig. 4). However, Schneider et al. (2017) reported an opposite tide between them, which might be a result of conspicuous differences in environmental conditions among cloud events. While there are some studies reporting the similar dependence of MSE and NSE of BC on supersaturation (Matsui, 2016; Motos et al., 2019a; Wu et al., 2019), the relationship between LWC and supersaturation is fairly complicated (Motos et al., 2019a; Pinsky et al., 2013).

Fig. 5 shows the correlations between the MSE of EBC and the EBC concentration, and between the NSE of BC and the number of BC-containing particles in cloud INT, respectively. Under a specific LWC condition (dots with the same color in Fig. 5), NSE to some extent decreased with the increasing number concentration of cloud INT, suggesting high concentration of particle hindered the incorporation into droplets due to the competition for the limited water vapor (Cozic et al., 2007). The trend became more obvious when we displayed an overview throughout the cloud event ($R^2$ are 0.66 and 0.88). Similar decreasing trend for MSE with increasing mass concentration of particles (or BC) was widely observed (Cozic et al., 2007; Gieray et al., 1997;

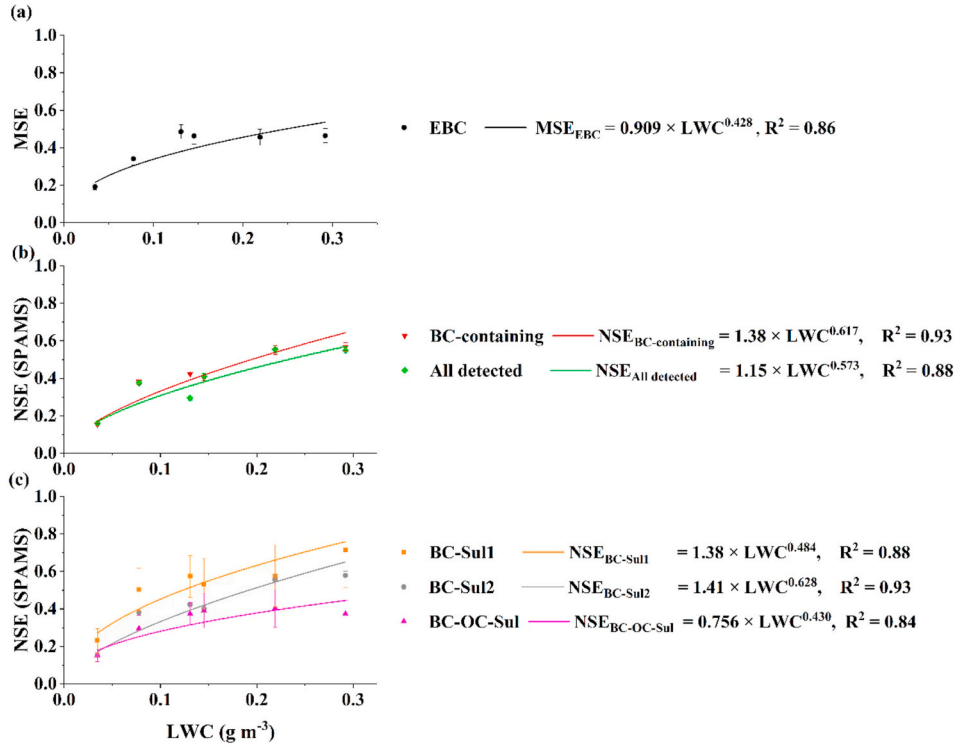


**Fig. 4.** Power fitting curves between LWC and SE of (a) mass of EBC by AE-33 and (b) and (c) particles by SPAMS, respectively.

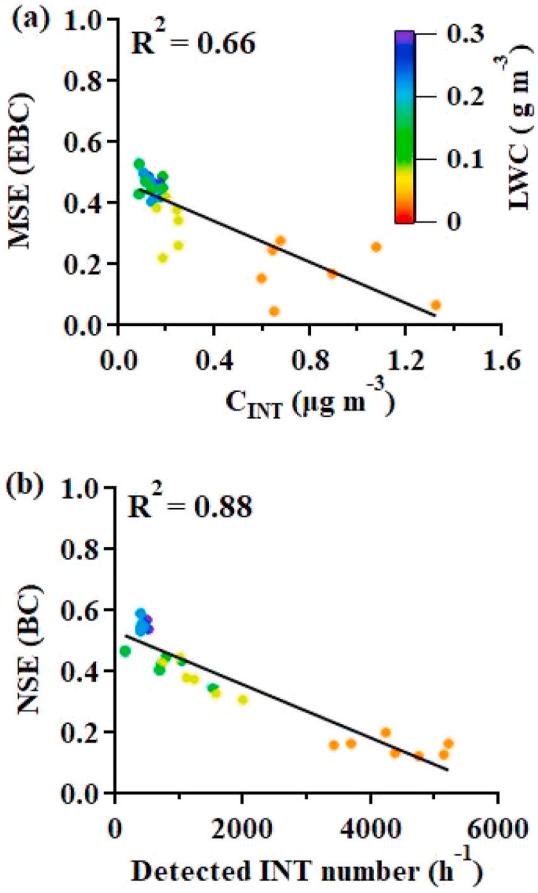


**Fig. 5.** (a) MSE of EBC as a function of cloud INT EBC mass concentration and (b) NSE of BC-containing particles as a function of detected number of cloud INT BC-containing particles. The color scale denotes the values of LWC. (For interpretation of the references to color in this figure legend, the reader is referred to the Web version of this article.)

Hallberg et al., 1994; Hallberg et al., 1992). Some exceptions, for instance, were found with no correlation between MSE and mass concentration of BC at Mt. Sonnblick (Hitzenberger et al., 2000; Kasper-Giebl et al., 2000) and Mt. Rax (Hitzenberger et al., 2001).

### 3.3.2. *Particle size and chemical composition*

Generally, fresh BC particles distribute in submicron range, however, aging processes can make them grow and internally mix with many compounds (Bond et al., 2013). It's better to understand the intrinsic relationship between MSE of EBC and particle size by using the core diameter than the diameter of cloud droplets (Motos et al., 2019a). Herein, stage-resolved relationships between NSEs of different types of BC-containing particles and $D_{va}$ of cloud RES particles are shown in Fig. 6. The NSEs of all types of particles increase with the growing $D_{va}$, indicating that larger particles are preferentially to be scavenged than smaller ones and nucleation was the primary mechanism of wet scavenging in this study in a size range of 0.4–1.2 μm, as discussed in our previous study, in which the size range is broader (0.1–1.6 μm) (Zhang et al., 2017). Hence, despite that the fraction of BC in the range of smaller than 40 nm ($D_m$) is unclear (Fig. 3), the impact of impaction/-coagulation processes on scavenging BC-containing particles detected by SPAMS can be ignored. The average $D_{va}$ of three stages (ranging from 0.69 to 0.79 μm) is the largest in the formation stage, followed by the dissipation stage and the development and stability stage (Fig. S7). Regarding the highest LWC in the development and stability stage, it's reasonable to infer that sufficient water vapor facilitated smaller particles to enter cloud droplets (Hoose et al., 2008). However, in the formation stage and the dissipation stages, low LWC did not facilitate the scavenging of smaller particles.

The influence of chemical compositions on the SEs of the BC-containing particles can be well reflected in Fig. 4 (c). While all the particle types of the BC-containing particles show a similar increasing trend towards LWC, the difference between SEs of different types can be as large as 30%. The maximum extent of increase was observed for BC-Sul1, followed by BC-Sul2 and BC-OC-Sul. Such a remarkable different dependence of NSEs on LWC could be attributed to the discrepancies of hygroscopicity. BC in type BC-Sul1 and BC-Sul2 have coatings with more water-soluble species (sulfate, nitrate, etc.) than the BC-OC-Sul type, with more organics. The hygroscopicity parameter kappas ($\kappa$) of sulfate (0.51–1.01) are considerably larger than those of organics (0.006–0.44) under sub-saturated conditions (Clegg and Brimblecombe, 1998; Koehler et al., 2006; Petters and Kreidenweis, 2007; Prenni et al., 2003). As BC-containing particles are highly aged, they become more hydrophilic than fresh emitted ones, and the hygroscopicity is highly dependent on the chemical compositions that are internally mixed with BC. There are studies reporting that the increased hygroscopicity of BC-containing particles could result in a similar scavenging behavior like bulk aerosols (Cozic et al., 2007; Zhang et al., 2017), and such phenomenon is also observed in the present study (Figs. 4 (b) and Fig. 6).

The NSE order is the same for three cloud stages but the discrepancies among various types are different (Fig. 6). Regarding BC-OC-Sul and BC-containing particles, the average NSE discrepancy is the lowest in the formation stage (0.1%) and the highest in the dissipation stage

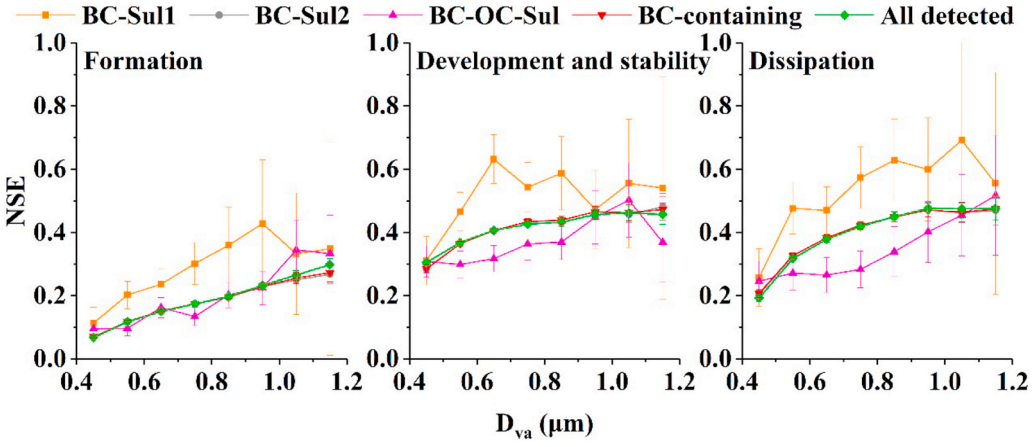


**Fig. 6.** Stage-resolved variation of NSEs of different types of detected particles with $D_{va}$. The error bars denote the standard deviation of NSE based on the hypothesis the NSE followed a Poisson's distribution.

(8.6%) while the largest discrepancy was observed at size bin of ~0.6–0.8 μm for each stage (with highest value of ~13% in the dissipation stage). The more considerable discrepancy may be attributed to slightly higher organics content existing at the size bin of 0.6–0.8 μm in cloud INT particles, hampering the particles to incorporate into cloud droplets (Fig. S6). Furthermore, the opposite trend between particle size and NSE was observed for three types of BC-containing particles (Fig. S7).

Considering organics are ubiquitous in the atmosphere and usually mixed with carbonous aerosols (namely BC-OC-Sul in the present study), we compared the SEs of organics with that of BC-OC-Sul. During the campaign, organic compounds (OC) and high molecular organic compounds (HMOC) were detected. OC particles were dominated by fragment ions of organics ($m/z$27 $C_2H_3^+$, 37 $C_3H^+$, 43 $C_2H_3O^+$, −26 $CN^-$, …) while HMOC by some other organic peaks (m/z77 $C_6H_5^+$, 91 $C_7H_7^+$) apart from those present in OC particles. Further, HMOC particles were distinguished from OC particles by marked ion fragments of $m/z > 100$ (Fig. S8) (Fu et al., 2020). OC and HMOC made up of 2.4% and 0.1% in cloud RES during the cloud event, respectively. It can be seen the size-resolved SEs of OC and HMOC were lower than BC-OC-Sul, suggesting that increasing organics would hinder particle scavenging (Fig. S9).

Besides, the variations of NSE of organics were also estimated. The NSE of organics (OC and HMOC) was lower than BC-containing particles, ranging from 2.1% to 65.0% with an average value of 16.0% throughout the cloud event. The average NSE was 7.6%, 33.0% and 13.3% for the three continuous cloud stages, respectively. It should be noted that the values may be overestimated for in-cloud formation of organics is prevalent.

The influence of convection on the in-cloud scavenging of particles have been considered in recent studies (Motos et al., 2019a; Xu et al., 2019). Xu et al. (2019) pointed out that convection scavenging shows the largest influence on BC mass concentration at mid-altitude region over tropics than the others. Motos et al. (2019a) revealed that updraft influence BC scavenging through the peak supersaturation ($SS_{peak}$). It's found that $SS_{peak}$ is positively corelate with updraft velocity and the increasing updraft velocity with increasing vertical distance from cloud base leads to higher $SS_{peak}$ above the cloud base than that at the cloud base (Hammer et al., 2015; Romakkaniemi et al., 2017). However, the relationship between LWC and $SS_{peak}$ remains unclear (Motos et al., 2019a; Pinsky et al., 2013), which limits us to estimate the impact of convection on BC scavenging.

Cloud boundary information might affect the interactions between ambient particles and LWC, since the hygroscopicity of ambient particles to a large extent determines whether they can serve as CCN (Väisänen et al., 2016). Besides, the mass concentration, size distribution and chemical composition for aerosols may be different outside (above, below and vicinity) and inside the cloud. Crumeyrolle et al. (2013) found the fraction of sulfate in aerosols markedly increased when approaching the cloud layer, facilitating them to incorporate into cloud. However, it remains a challenge to obtain cloud boundary information during the orographic cloud observations (Pratt et al., 2010; Roth et al., 2016). Also, in our in-situ measurements, we didn't get information about cloud boundary and such issue calls for further investigation.

Apart from the factors mentioned above, morphology may be a momentous factor, either. Generally, BC undergone cloud processing would become more compact (Bhandari et al., 2019), whereas our morphology study on soot (BC) during cloud events at this site showed that interstitial particles were more compact and less branched than cloud residue particles (Fu et al., 2020). These phenomena may impact BC scavenging but need further investigations.

### 3.4. Key influencing factor on SE of BC-containing particles in different cloud stages

As discussed above, the SEs of submicron particles and BC-containing particles are strongly dependent on LWC. At a specific size bin, the NSE varied significantly with the cloud stages, which also meant a good correlation with LWC. Thus, it's reasonable to infer LWC is the most critical factor in determining the SE of BC-containing particles throughout the cloud event.

Considering that the increase of NSE with particle size was commonly observed even for type BC-OC-Sul, and that chemical composition didn't show considerable variation throughout the cloud event, the influence of size on NSE may dominate over chemical composition. At the formation stage, LWC was relatively low, and the smallest difference was observed among three types of particles compared to the other two stages, indicating a limited influence of LWC and chemical composition on SE. At this stage, mass/number concentration of the INT particles was dramatically high, hence those particles with larger sizes take more chances to incorporate into the cloud. In other words, particle size takes an overwhelming advantage in influencing the SE of BC-containing particles.

When the cloud was stable, sufficient LWC made particle size to be a minor contributor for in-cloud scavenging. We noted that during 0:00–8:00 on 1, Jun, the SEs increased remarkably (ΔSE was 39.5% for mass and 31.1% for number, respectively) while the LWC was not the highest (0.13 g $m^{-3}$). Oppositely, smaller variations of SEs were observed (ΔSE is 11.9% for mass and 24.8% for number, respectively) when LWC varied from 0.13 to 0.29 g $m^{-3}$ (Fig. 2), indicating that LWC was not the decisive factor in this stage. Besides, the discrepancies of NSEs among three types of BC-containing particles became increasingly evident throughout the cloud event (Fig. 6), highlighting the increasing role of chemical composition.

When the cloud tended to dissipate, the fact that SEs fell gently and the LWC decreased dramatically indicates a light impact of LWC on SE. Furthermore, the NSEs increased fastest with particle size, and the discrepancies of NSEs among different types are the largest in this stage (Fig. 6), indicating that size and chemical composition may be momentous at the dissipation stage.

## 4. Conclusions

The evolution of SE of BC and the stage-resolved main influencing factors were firstly investigated. The MSE of EBC and NSE of BC-containing particles varied from 4.7% to 52.6% and 11.3%–59.6%, with a mean value of 35.1% and 37.3%, respectively. The SEs were the highest in the development and stability stage, followed by the dissipation stage and the formation stage, respectively. The NSEs of different types of particles increased with particle size (0.4–1.2 μm) and LWC, despite the fact that organics coated type particles were less scavenged compared to sulfate coated types. Submicron particles (20–620 nm) scavenging was dominated by coagulation/impaction for 20–30 nm size bin and nucleation for > 50 nm size bins. Based on the stage-resolved and comprehensive analysis, we infer that LWC is the predominant factor in determining the SEs of BC-containing particles throughout the cloud event. Other key factors influencing SE of BC are particle size for the formation stage, chemical composition for the development and stability stage, both particle size and chemical composition for the dissipation stage, respectively. The present results may provide a crucial constrain for wet scavenging of BC in modelling investigations.

## CRediT authorship contribution statement

**Yuxiang Yang:** Writing - review & editing, Funding acquisition, Writing - original draft. **Qinhao Lin:** Formal analysis. **Yuzhen Fu:** Formal analysis. **Xiufeng Lian:** Software, Validation. **Feng Jiang:** Software, Validation. **Long Peng:** Software, Validation. **Guohua Zhang:**

Writing - review & editing, Funding acquisition, Methodology, Resources, Writing - original draft, Conceptualization. **Lei Li:** Methodology, Resources. **Duohong Chen:** Formal analysis, Formal analysis, Formal analysis, Methodology, Resources. **Mei Li:** Methodology, Resources. **Jie Ou:** Methodology, Resources. **Xinhui Bi:** Conceptualization, Supervision, Writing - original draft, Writing - review & editing, Funding acquisition. **Xinming Wang:** Methodology, Resources. **Guoying Sheng:** Methodology, Resources.

## Declaration of competing interest

The authors declare that they have no known competing financial interests or personal relationships that could have appeared to influence the work reported in this paper.

## Acknowledgments

This work was supported by the National Nature Science Foundation of China (No. 41775124 and 41877307), Natural Science Foundation of Guangdong Province (2019B151502022), the National Key Research and Development Program of China (2017YFC0210104), and Guangdong Foundation for Program of Science and Technology Research (No. 2017B030314057). The authors also gratefully acknowledge the NOAA Air Resources Laboratory (ARL) for the provision of the HYSPLIT transport and dispersion model (http://ready.arl.noaa.gov) used in this publication.

## Appendix A. Supplementary data

Supplementary data to this article can be found online at https://doi.org/10.1016/j.atmosenv.2020.117883.

## References

Acker, K., Mertes, S., Moller, D., Wieprecht, W., Auel, R., Kalass, D., 2002. Case study of cloud physical and chemical processes in low clouds at Mt. Brocken. Atmos. Res. 64, 41–51.

Baumgardner, D., Subramanian, R., Twohy, C., Stith, J., Kok, G., 2008. Scavenging of black carbon by ice crystals over the northern Pacific. Geophys. Res. Lett. 35, 1–5.

Bhandari, J., China, S., Chandrakar, K.K., Kinney, G., Cantrell, W., Shaw, R.A., Mazzoleni, L.R., Girotto, G., Sharma, N., Gorkowski, K., Gilardoni, S., Decesari, S., Facchini, M.C., Zanca, N., Pavese, G., Esposito, F., Dubey, M.K., Aiken, A.C., Chakrabarty, R.K., Moosmuller, H., Onasch, T.B., Zaveri, R.A., Scarnato, B.V., Fialho, P., Mazzoleni, C., 2019. Extensive soot compaction by cloud processing from laboratory and field observations. Sci. Rep. 9, 11824.

Bi, X., Lin, Q., Peng, L., Zhang, G., Wang, X., Brechtel, F.J., Chen, D., Li, M., Peng, P., Sheng, G., Zhou, Z., 2016. In situ detection of the chemistry of individual fog droplet residues in the Pearl River Delta region, China. J. Geophys. Res. 121, 9105–9116.

Bond, T.C., Doherty, S.J., Fahey, D.W., Forster, P.M., Berntsen, T., DeAngelo, B.J., Flanner, M.G., Ghan, S., Kärcher, B., Koch, D., Kinne, S., Kondo, Y., Quinn, P.K., Sarofim, M.C., Schultz, M.G., Schulz, M., Venkataraman, C., Zhang, H., Zhang, S., Bellouin, N., Guttikunda, S.K., Hopke, P.K., Jacobson, M.Z., Kaiser, J.W., Klimont, Z., Lohmann, U., Schwarz, J.P., Shindell, D., Storelvmo, T., Warren, S.G., Zender, C.S., 2013. Bounding the role of black carbon in the climate system: a scientific assessment. J. Geophys. Res. 118, 5380–5552.

Browse, J., Carslaw, K.S., Arnold, S.R., Pringle, K., Boucher, O., 2012. The scavenging processes controlling the seasonal cycle in Arctic sulphate and black carbon aerosol. Atmos. Chem. Phys. 12, 6775–6798.

Ching, J., Riemer, N., West, M., 2012. Impacts of black carbon mixing state on black carbon nucleation scavenging: insights from a particle-resolved model. J. Geophys. Res. 117.

Ching, J., West, M., Riemer, N., 2018. Quantifying impacts of aerosol mixing state on nucleation-scavenging of black carbon aerosol particles. Atmosphere 9, 1–17.

Clegg, S.L., Brimblecombe, P., 1998. Thermodynamic model of the system $H^+$–$NH_4^+$–Na$^+$–$SO_4^{2-}$–$NO_3^-$–$Cl^-$–$H_2O$ at 298.15 K. J. Phys. Chem. 2155–2171.

Cozic, J., Verheggen, B., Mertes, S., Connolly, P., Bower, K., Petzold, A., Baltensperger, U., Weingartner, E., 2007. Scavenging of black carbon in mixed phase clouds at the high alpine site Jungfraujoch. Atmos. Chem. Phys. 7, 1797–1807.

Croft, B., Martin, R.V., Leaitch, W.R., Tunved, P., Breider, T.J., D'Andrea, S.D., Pierce, J. R., 2016. Processes controlling the annual cycle of Arctic aerosol number and size distributions. Atmos. Chem. Phys. 16, 3665–3682.

Crumeyrolle, S., Weigel, R., Sellegri, K., Roberts, G., Gomes, L., Stohl, A., Laj, P., Momboisse, G., Bourianne, T., Puygrenier, V., Burnet, F., Chosson, F., Brenguier, J. L., Etcheberry, J.M., Villani, P., Pichon, J.M., Schwarzenboeck, A., 2013. Airborne investigation of the aerosols–cloud interactions in the vicinity and within a marine stratocumulus over the North Sea during EUCAARI (2008). Atmos. Environ. 81, 288–303.

Demoz, B.B., Collett, J.L., Daube, B.C., 1996. On the caltech active strand cloudwater collectors. Atmos. Res. 41, 47–62.

Ding, S., Zhao, D., He, C., Huang, M., He, H., Tian, P., Liu, Q., Bi, K., Yu, C., Pitt, J., Chen, Y., Ma, X., Chen, Y., Jia, X., Kong, S., Wu, J., Hu, D., Hu, K., Ding, D., Liu, D., 2019. Observed interactions between black carbon and hydrometeor during wet scavenging in mixed-phase clouds. Geophys. Res. Lett. 46, 8453–8463.

Drinovec, L., Močnik, G., Zotter, P., Prévôt, A.S.H., Ruckstuhl, C., Coz, E., Rupakheti, M., Sciare, J., Müller, T., Wiedensohler, A., Hansen, A.D.A., 2015. The "dual-spot" Aethalometer: an improved measurement of aerosol black carbon with real-time loading compensation. Atmos. Meas. Tech. 8, 1965–1979.

Dupont, J.C., Haeffelin, M., Protat, A., Bouniol, D., Boyouk, N., Morille, Y., 2012. Stratus–Fog formation and dissipation: a 6-day case study. Bound. Layer Meteorol 143, 207–225.

Emerson, E.W., Katich, J.M., Schwarz, J.P., McMeeking, G.R., Farmer, D.K., 2018. Direct measurements of dry and wet deposition of black carbon over a grassland. J. Geophys. Res. 123, 12277–12290.

Ervens, B., 2015. Modeling the processing of aerosol and trace gases in clouds and fogs. Chem. Rev. 115, 4157–4198.

Fu, Y., Lin, Q., Zhang, G., Yang, Y., Yang, Y., Lian, X., Peng, L., Jiang, F., Bi, X., Li, L., Wang, Y., Chen, D., Ou, J., Wang, X., Peng, P., Zhu, J., Sheng, G., 2020. Impact of in-cloud aqueous processes on the chemical compositions and morphology of individual atmospheric aerosols. Atmos. Chem. Phys. Discuss. https://doi.org/10.5194/acp-2020-373. In press.

Gieray, R., Wieser, P., Engelhardt, T., 1997. Phase partitioning of aerosol constitutents in cloud based on single-particle and bulk analysis. Atmos. Environ. 31, 2491–2502.

Guo, J., Wang, Y., Shen, X.H., Wang, Z., Lee, T., Wang, X.F., Li, P.H., Sun, M.H., Collett, J.L., Wang, W.X., Wang, T., 2012. Characterization of cloud water chemistry at Mount Tai, China: seasonal variation, anthropogenic impact, and cloud processing. Atmos. Environ. 60, 467–476.

Hallberg, A., Noone, K.J., Ogren, J.A., Svenningsson, I.B., Flossmann, A., Wiedensohler, A., Hansson, H.C., Heintzenberg, J., Anderson, T.L., Arends, B.G., Maser, R., 1994. Phase partitioning of aerosol-particles in clouds at Kleiner-Feldberg. J. Atmos. Chem. 19, 107–127.

Hallberg, A., Organ, J.A., Noone, K.J., Heintenberg, J., 1992. Phase partitioning for different aerosol spcies in fog. Tellus B 44, 545–555.

Hammer, E., Bukowiecki, N., Luo, B.P., Lohmann, U., Marcolli, C., Weingartner, E., Baltensperger, U., Hoyle, C.R., 2015. Sensitivity estimations for cloud droplet formation in the vicinity of the high-alpine research station Jungfraujoch (3580 m a.s.l.). Atmos. Chem. Phys. 15, 10309–10323.

Heintzenberg, J., Cereceda-Balic, F., Vidal, V., Leck, C., 2016. Scavenging of black carbon in Chilean coastal fogs. Sci. Total Environ. 541, 341–347.

Heintzenberg, J., Leck, C., 1994. Seasonal variation of the atmospheric aerosol near the top of the marine boundary layer over Spitsbergen related to the Arctic sulphur cycle. Tellus B 46, 52–67.

Henning, S., Weingartner, E., Schmidt, S., Wendisch, M., Gaggeler, H.W., Baltensperger, U., 2002. Size-dependent aerosol activation at the high-alpine site Jungfraujoch (3580 m a.s.l.). Tellus B 54, 82–95.

Herckes, P., Valsaraj, K.T., Collett, J.L., 2013. A review of observations of organic matter in fogs and clouds: origin, processing and fate. Atmos. Res. 132, 434–449.

Hitzenberger, R., Berner, A., Glebl, H., Drobesch, K., Kasper-Giebl, A., Loeflund, M., Urban, H., Puxbaum, H., 2001. Black carbon (BC) in alpine aerosols and cloud water - concentrations and scavenging efficiencies. Atmos. Environ. 35, 5135–5141.

Hitzenberger, R., Berner, A., Kromp, R., Kasper-Giebl, A., Limbeck, A., Tscherwenka, W., Puxbaum, H., 2000. Black carbon and other species at a high-elevation European site (Mount Sonnblick, 3106 m, Austria): concentrations and scavenging efficiencies. J. Geophys. Res. 105, 24637–24645.

Hoose, C., Lohmann, U., Stier, P., Verheggen, B., Weingartner, E., 2008. Aerosol processing in mixed-phase clouds in ECHAM5-HAM: model description and comparison to observations. J. Geophys. Res. 113.

Jurado, E., Dachs, J., Duarte, C.M., Simo, R., 2008. Atmospheric deposition of organic and black carbon to the global oceans. Atmos. Environ. 42, 7931–7939.

Kasper-Giebl, A., Koch, A., Hitzenberger, R., Puxbaum, H., 2000. Scavenging efficiency of 'aerosol carbon' and sulfate in supercooled clouds at Mt. Sonnblick (3106 m a.s.l., Austria). J. Atmos. Chem. 35, 33–46.

Koch, D., Del Genio, A.D., 2010. Black carbon semi-direct effects on cloud cover: review and synthesis. Atmos. Chem. Phys. 10, 7685–7696.

Koehler, K.A., Kreidenweis, S.M., DeMott, P.J., Prenni, A.J., Carrico, C.M., Ervens, B., Feingold, G., 2006. Water activity and activation diameters from hygroscopicity data - Part II: application to organic species. Atmos. Chem. Phys. 6, 795–809.

Koracin, D., Businger, J., Dorman, C., Lewis, J., 2005. Formation, evolution, and dissipation of coastal sea fog. Bound. Layer Meteorol. 117, 447–478.

Levin, Z., Teller, A., Ganor, E., Graham, B., Andreae, M.O., Maenhaut, W., Falkovich, A. H., Rudich, Y., 2003. Role of aerosol size and composition in nucleation scavenging within clouds in a shallow cold front. J. Geophys. Res. 108.

Li, L., Huang, Z.X., Dong, J.G., Li, M., Gao, W., Nian, H.Q., Fu, Z., Zhang, G.H., Bi, X.H., Cheng, P., Zhou, Z., 2011. Real time bipolar time-of-flight mass spectrometer for analyzing single aerosol particles. Int. J. Mass Spectrom. 303, 118–124.

Lin, Q., Zhang, G., Peng, L., Bi, X., Wang, X., Brechtel, F.J., Li, M., Chen, D., Peng, P., Sheng, G., Zhou, Z., 2017. In situ chemical composition measurement of individual cloud residue particles at a mountain site, southern China. Atmos. Chem. Phys. 17, 8473–8488.

Liu, L., Zhang, J., Xu, L., Yuan, Q., Huang, D., Chen, J., Shi, Z., Sun, Y., Fu, P., Wang, Z., Zhang, D., Li, W., 2018. Cloud scavenging of anthropogenic refractory particles at a mountain site in North China. Atmos. Chem. Phys. 18, 14681–14693.

Matsui, H., 2016. Black carbon simulations using a size- and mixing-state-resolved three-dimensional model: 2. Aging timescale and its impact over East Asia. J. Geophys. Res. 121, 1808–1821.
Moteki, N., Kondo, Y., Oshima, N., Takegawa, N., Koike, M., Kita, K., Matsui, H., Kajino, M., 2012. Size dependence of wet removal of black carbon aerosols during transport from the boundary layer to the free troposphere. Geophys. Res. Lett. 39, 13801–13804. L13802.
Motos, G., Schmale, J., Corbin, J.C., Modini, R.L., Karlen, N., Bertò, M., Baltensperger, U., Gysel-Beer, M., 2019a. Cloud droplet activation properties and scavenged fraction of black carbon in liquid-phase clouds at the high-alpine research station Jungfraujoch (3580 m a.s.l.). Atmos. Chem. Phys. 19, 3833–3855.
Motos, G., Schmale, J., Corbin, J.C., Zanatta, M., Baltensperger, U., Gysel-Beer, M., 2019b. Droplet activation behaviour of atmospheric black carbon particles in fog as a function of their size and mixing state. Atmos. Chem. Phys. 19, 2183–2207.
Nordmann, S., Cheng, Y.F., Carmichael, G.R., Yu, M., van der Gon, H.A.C.D., Zhang, Q., Saide, P.E., Poschl, U., Su, H., Birmili, W., Wiedensohler, A., 2014. Atmospheric black carbon and warming effects influenced by the source and absorption enhancement in central Europe. Atmos. Chem. Phys. 14, 12683–12699.
Ohata, S., Moteki, N., Mori, T., Koike, M., Kondo, Y., 2016. A key process controlling the wet removal of aerosols: new observational evidence. Sci. Rep. 6, 34113.
Petters, M.D., Kreidenweis, S.M., 2007. A single parameter representation of hygroscopic growth and cloud condensation nucleus activiity. Atmos. Chem. Phys. 7, 1961–1971.
Petzold, A., Ogren, J.A., Fiebig, M., Laj, P., Li, S.M., Baltensperger, U., Holzer-Popp, T., Kinne, S., Pappalardo, G., Sugimoto, N., Wehrli, C., Wiedensohler, A., Zhang, X.Y., 2013. Recommendations for reporting "black carbon" measurements. Atmos. Chem. Phys. 13, 8365–8379.
Pierce, J.R., Croft, B., Kodros, J.K., D'Andrea, S.D., Martin, R.V., 2015. The importance of interstitial particle scavenging by cloud droplets in shaping the remote aerosol size distribution and global aerosol-climate effects. Atmos. Chem. Phys. 15, 6147–6158.
Pinsky, M., Mazin, I.P., Korolev, A., Khain, A., 2013. Supersaturation and diffusional droplet growth in liquid clouds. J. Atmos. Sci. 70, 2778–2793.
Pratt, K.A., Twohy, C.H., Murphy, S.M., Moffet, R.C., Heymsfield, A.J., Gaston, C.J., DeMott, P.J., Field, P.R., Henn, T.R., Rogers, D.C., Gilles, M.K., Seinfeld, J.H., Prather, K.A., 2010. Observation of playa salts as nuclei in orographic wave clouds. J. Geophys. Res. 115.
Prenni, A.J., De Mott, P.J., Kreidenweis, S.M., 2003. Water uptake of internally mixed particles containing ammonium sulfate and dicarboxylic acids. Atmos. Environ. 37, 4243–4251.
Psichoudaki, M., Nenes, A., Florou, K., Kaltsonoudis, C., Pandis, S.N., 2018. Hygroscopic properties of atmospheric particles emitted during wintertime biomass burning episodes in Athens. Atmos. Environ. 178, 66–72.
Romakkaniemi, S., Maalick, Z., Hellsten, A., Ruuskanen, A., Väisänen, O., Ahmad, I., Tonttila, J., Mikkonen, S., Komppula, M., Kühn, T., 2017. Aerosol–landscape–cloud interaction: signatures of topography effect on cloud droplet formation. Atmos. Chem. Phys. 17, 7955–7964.
Roth, A., Schneider, J., Klimach, T., Mertes, S., van Pinxteren, D., Herrmann, H., Borrmann, S., 2016. Aerosol properties, source identification, and cloud processing in orographic clouds measured by single particle mass spectrometry on a central European mountain site during HCCT-2010. Atmos. Chem. Phys. 16, 505–524.
Schneider, J., Mertes, S., van Pinxteren, D., Herrmann, H., Borrmann, S., 2017. Uptake of nitric acid, ammonia, and organics in orographic clouds: mass spectrometric analyses of droplet residual and interstitial aerosol particles. Atmos. Chem. Phys. 17, 1571–1593.
Schroder, J.C., Hanna, S.J., Modini, R.L., Corrigan, A.L., Kreidenwies, S.M., Macdonald, A.M., Noone, K.J., Russell, L.M., Leaitch, W.R., Bertram, A.K., 2015. Size-resolved observations of refractory black carbon particles in cloud droplets at a marine boundary layer site. Atmos. Chem. Phys. 15, 1367–1383.
Sellegri, K., Laj, P., Dupuy, R., Legrand, M., Preunkert, S., Putaud, J.P., 2003. Size-dependent scavenging efficiencies of multicomponent atmospheric aerosols in clouds. J. Geophys. Res. 108.
Shingler, T., Dey, S., Sorooshian, A., Brechtel, F.J., Wang, Z., Metcalf, A., Coggon, M., Mulmenstadt, J., Russell, L.M., Jonsson, H.H., Seinfeld, J.H., 2012. Characterisation and airborne deployment of a new counterflow virtual impactor inlet. Atmos. Meas. Tech. 5, 1259–1269.
Targino, A.C., Coe, H., Cozic, J., Crosier, J., Crawford, I., Bower, K., Flynn, M., Gallagher, M., Allan, J., Verheggen, B., Weingartner, E., Baltensperger, U., Choularton, T., 2009. Influence of particle chemical composition on the phase of cold clouds at a high-alpine site in Switzerland. J. Geophys. Res. 114.
Targino, A.C., Noone, K.J., Drewnick, F., Schneider, J., Krejci, R., Olivares, G., Hings, S., Borrmann, S., 2007. Microphysical and chemical characteristics of cloud droplet residuals and interstitial particles in continental stratocumulus clouds. Atmos. Res. 86, 225–240.
Taylor, J.W., Allan, J.D., Allen, G., Coe, H., Williams, P.I., Flynn, M.J., Le Breton, M., Muller, J.B.A., Percival, C.J., Oram, D., Forster, G., Lee, J.D., Rickard, A.R., Parrington, M., Palmer, P.I., 2014. Size-dependent wet removal of black carbon in Canadian biomass burning plumes. Atmos. Chem. Phys. 14, 13755–13771.
Väisänen, O., Ruuskanen, A., Ylisirniö, A., Miettinen, P., Portin, H., Hao, L., Leskinen, A., Komppula, M., Romakkaniemi, S., Lehtinen, K.E.J., Virtanen, A., 2016. In-cloud measurements highlight the role of aerosol hygroscopicity in cloud droplet formation. Atmos. Chem. Phys. 16, 10385–10398.
Wu, Y., Liu, D., Wang, J., Shen, F., Chen, Y., Cui, S., Ge, S., Wu, Y., Chen, M., Ge, X., 2019. Characterization of size-resolved hygroscopicity of black carbon-containing particle in urban environment. Environ. Sci. Technol. 53, 14212–14221.
Xu, J., Zhang, J., Liu, J., Yi, K., Xiang, S., Hu, X., Wang, Y., Tao, S., Ban-Weiss, G., 2019. Influence of cloud microphysical processes on black carbon wet removal, global distributions, and radiative forcing. Atmos. Chem. Phys. 19, 1587–1603.
Yang, Y., Fu, Y., Lin, Q., Jiang, F., Lian, X., Li, L., Wang, Z., Zhang, G., Bi, X., Wang, X., Sheng, G., 2019. Recent advances in quantifying wet scavenging efficiency of black carbon aerosol. Atmosphere 10, 175.
Zhang, G., Lin, Q., Peng, L., Bi, X., Chen, D., Li, M., Li, L., Brechtel, F.J., Chen, J., Yan, W., Wang, X., Peng, P., Sheng, G., Zhou, Z., 2017. The single-particle mixing state and cloud scavenging of black carbon: a case study at a high-altitude mountain site in southern China. Atmos. Chem. Phys. 17, 14975–14985.